P25 and Rutile Titania in Photocatalytic Degradation of Phenol and Methylene Blue

Ana L.R. Melo, Maria F.R. Sachi, Zuy M Magriotis, Natália M.B. Oliveira, and Cristiane A. Pereira*.
Laboratory of Catalysis and Biofuels, Department of Chemical and Materials Engineering, School of Engineering, Federal University of Lavras, P. O. Box 3037, CEP 37203-202, Lavras, MG, Brazil. Ana L.R. Melo (e-mail: ana.melo4@estudante.ufla.br). Maria F.R. Sacchi (e-mail: maria.sachi@estudante.ufla.br). Zuy M. Magriotis (e-mail: zuy@ufla.br). Natália M.B. Oliveira (e-mail: natalia.boliveira@ufla.br). Cristiane A. Pereira (e-mail: cristiane.alpereira@ufla.br)

DOI: https://doi.org/10.34024/jsse.2024.v2.19413

***Abstract*— Phenolic compounds, dyes, and their derivatives are prevalent organic pollutants in surface waters due to industrial activities, effluent discharge, and agricultural runoff. In this context, this study aimed to evaluate the photocatalytic activity of commercial P25 TiO_2 (TiO_2-P25) and rutile TiO_2 (TiO_2-R) solids for the degrading phenol and methylene blue dye in a batch reactor under UV-C irradiation at 256 nm. X-ray diffraction data confirm the predominant presence of the anatase phase in TiO_2-P25 and the rutile phase in TiO_2-R. Significant difference in crystallite size and specific area (S_{BET}) between the samples were linked to their commercial synthesis method. The results demonstrated that TiO_2-P25 exhibited higher photocatalytic activity than TiO_2-R due to differences in band gap. The use of a 15W lamp further enhanced this efficiency. For phenol degradation, TiO_2-P25 obtained 57% conversion at 9W and an 11% increase in the initial concentration at 15W, while TiO_2-R showed lower efficiency. In photolysis, minimal conversion was observed. Total organic carbon (TOC) data suggest that photocatalysis generates organic metabolites rather than achieving complete mineralization, leading to the accumulation of intermediates in the effluent, particularly with the 15W lamp.**

***Keywords*— AOPs, photocatalyst, pollution control, titanium dioxide.**

I. Introduction

Industrial advancement has been crucial in the economic and technological development of society. However, this progress has also led to major environmental challenges, particularly the contamination of aquatic systems by organic compounds such as pesticides, antibiotics, pharmaceuticals, and dyes [1], [2], [3], [4], [5]. Industrial wastewaters often contain pollutants and residues that are resistant to conventional treatment methods, posing serious risks to both human health and the environment [6]. Among these contaminants, phenol is particularly concerning due to its high toxicity and persistence in the environment, once it is widely applied in the production of plastics, detergents, medicines, and herbicides [7], [8]. Additionally, dyes from the textile industry, such as methylene blue (MB), pose a significant threat to aquatic ecosystems. These dyes not only produce effluents highly recalcitrant, but also obstruct the penetration of sunlight, leading to a decrease in oxygen concentration, which further endangers aquatic life and human health [9], [10].

Within this scenario, the advanced oxidative processes (AOPs) have emerged as a viable and promising alternative for the degradation of persistent organic contaminants, due to their high redox potential [11], [12]. Among these processes, attention has been given to heterogeneous photocatalysis, which is receiving great attention. This process utilizes sunlight or artificial light to activate catalysts, thereby enhancing chemical reactions [13]. The catalysts, acting as semiconductors, absorb photons upon light exposure, leading to electronic excitation from the valence band to the conduction band, which facilitates the formation of hydroxyl radicals and superoxide [14]. These radicals promote the fast degradation of persistent pollutants as they can chemically oxidize most non-biodegradable organic compounds, converting them into more easily degradable or inert substances such as water and carbon dioxide [14].

Typical photocatalysts include salts, sulfides, and metal oxides such as ZnS, AgCl, and ZnO [13], [15], [16]. Among these, titanium dioxide (or TiO_2) is notable for its efficiency, chemical stability, low toxicity, and cost-effectiveness [17]. TiO_2 exists in three crystalline forms: rutile (the most stable phase), anatase, and brookite, with the anatase and rutile phases the most relevant in catalysis [16]. The anatase crystal structure exhibits superior photocatalytic activity due to higher affinity for hydroxyl groups and lower carriers' recombination rate, whereas rutile is less effective because of larger grain size and reduced surface area [18]. Nonetheless, TiO_2 faces limitations including its high band gap energy (3.2 eV for anatase and 3.0 eV for rutile). However, synthesis methods, such as doping and incorporation of TiO_2 into mixed oxide composites can enhance its photocatalytic performance [19].

Doping of TiO_2 with nitrogen or metals, such as iron and silver, has been shown to significantly enhance the degradation of phenol and methylene blue [16], [20], [21], [22], [23], [24]. Additionally, TiO_2 composites incorporating materials like activated carbon, have optimized the photocatalytic oxidation

The paper was submitted for review on August 30, 2024. And this work was supported in part by the Minas Gerais Research Foundation (FAPEMIG).

of these contaminants due to the high surface area of the composite [25], [26]. However, for the effective application of these techniques, considering the development of innovative photocatalysts, it is essential to evaluate the influence of the crystalline phases of TiO_2 besides the intensity of radiation. So, based on these several aspects, this study investigated the photocatalytic activity of commercial P25 TiO_2-P25 (75% anatase and 25% rutile) and rutile phase TiO_2 in phenol and MB degradation. The conversion of organic compounds was analyzed by UV-vis spectrophotometry and compared with total organic carbon content (TOC) data. The photocatalysts were characterized by X-ray diffraction (XRD), Nitrogen adsorption-desorption measurements, and ultraviolet and visible diffuse reflectance spectroscopy ($DRS_{UV\text{-}vis}$), including band gap determination.

II. Experimental

A. Samples

TiO_2 P25 Aeroxide (TiO_2-P25) from Acros Organics and rutile-phase TiO_2 (TiO_2-R) from Didatica were applied as photocatalysts and used as received.

B. Characterization of photocatalysts

XRD data were used to confirm the crystalline structures present in each sample and to determine crystallite sizes [27]. The analyses used a Rigaku diffractometer with a Cu tube and Ni filters, operating with CuKα radiation (λ=0.1542 nm). The goniometer was set to a scanning speed of 2° 2θ min^{-1}, with an angle range from 10 to 70° (2θ).

Nitrogen adsorption-desorption measurements were performed at the boiling point of liquid nitrogen (-196 °C) in Micromeritics equipment. Before each analysis, the samples were pretreated at 200 °C for 2 h under vacuum to remove any adsorbed water. The specific surface area (S_{BET}) was calculated by the Brunauer-Emmet-Teller equation [28].

$DRS_{UV\text{-}vis}$ measurements were conducted using a Varian spectrophotometer and a $BaSO_4$ as a reference. Data were collected in the wavelength range between 220 and 800 nm, and the reflectance spectra were converted with the Kubelka-Munk function (F(R)), as given in (1), where R represents the diffuse reflectance of the material.

$$F(R) = 100\frac{(1-R)^2}{2R} \qquad (1)$$

The band gap values of the materials were determined by extrapolating a straight line fitted to the x-axis in a plot of $[F(R) \; x \; h\nu]^2$ by hν [29]. Here, F(R) represents the Kubelka-Munk function and hν denotes the energy of the incident photon.

C. Photocatalytic tests

Catalytic photodegradation tests of phenol or MB were conducted in a batch reactor (350 mL) within a sealed reaction chamber to prevent ambient light interference. In each photocatalytic experiment, 100 mL of an aqueous solution containing 100 ppm of phenol, or 30 ppm of MB was mixed with 0.1 g of TiO_2-P25 or TiO2-R and stirred in the absence of light for 2 h for phenol or 0.5 h for MB. The dark stirring time was chosen to reach adsorption equilibrium with the organic molecules. Subsequently, the solution was irradiated for 3 h using a 9 W or 15 W Phillips lamp (UV-C radiation, λ = 256 nm). Aliquots of 1 mL were collected from the reactor at established time intervals. After centrifugation, the samples were analyzed using a UV-vis spectrophotometer (Genesys 10S Thermo Scientific) at 269 nm for phenol degradation or a visible spectrophotometer (Bel V-M5) at 664 nm for MB. Photolysis tests, conducted under the same conditions but without photocatalysts, were conducted under the same reaction conditions, excluding the dark stirring step. The phenol or MB conversion (%), at each established reaction time t, was calculated as shown in (2), comparing the organic compound concentration (C) with its initial value (C_0).

$$Conversion, X = 100\frac{(C_0-C)}{C_0} \qquad (2)$$

To determine the content of organic compounds in each reaction effluent obtained after 3 h, total organic carbon (TOC) measurements were performed using a TOC-VCPH (SHIMADZU) analyzer, which employs the catalytic combustion oxidation method at 680 ºC.

III. RESULTS

A. Characterization

Fig. 1 shows the X-ray diffractograms between 20 and 70° (2θ) of the photocatalysts under study. Following the technical specifications, TiO_2-P25 exhibits both anatase and rutile crystalline phases. The peaks at 2θ equal to 25.5°, 37.2º, 38.1º, 48.3º, 54.1º and 62.9° correspond to diffraction in the crystal planes (101), (103), (004), (200), (105) and (204) of the anatase phase, while peaks at 2θ values 27.7º; 36.4º and 69.2° are attributed to diffraction in the (110), (101) and (301) planes for rutile titania. [JCPDS 78-2485; 84-1286]. For TiO_2-R, X-ray diffraction is observed at 2θ values of 27.7º; 36.4º; 39.3º, 41.4º; 44.1º, 54.5°, 56.7°, 62.9°, 64.2 and 69.2°, which are associated with the diffraction in the planes (110), (101), (200), (111), (210), (220), (211), (002), (310) and (301) of rutile phase [JCPDS 84-1286] [30]. Despite the predominance of rutile-related peaks in TiO_2-R, the diffractogram also presents minor signals at 2θ values of 25.5° and 48.3°, corresponding to the diffraction in the (101) and (200) crystalline planes of the anatase phase.

Table 1 provides the crystallite sizes of TiO_2-P25 and TiO_2-R, calculated using the Scherrer equation. There is a notable difference in the crystallite sizes, which can be related to the commercial synthesis method of the samples, including variations in heat treatment temperatures. When P25 titanium dioxide was analyzed by thermogravimetry and differential thermal analysis (DTA), an exothermic event was observed,

indicating that the transition from anatase to rutile occurs gradually as the temperature increases, beginning around 350 °C [31], [32].

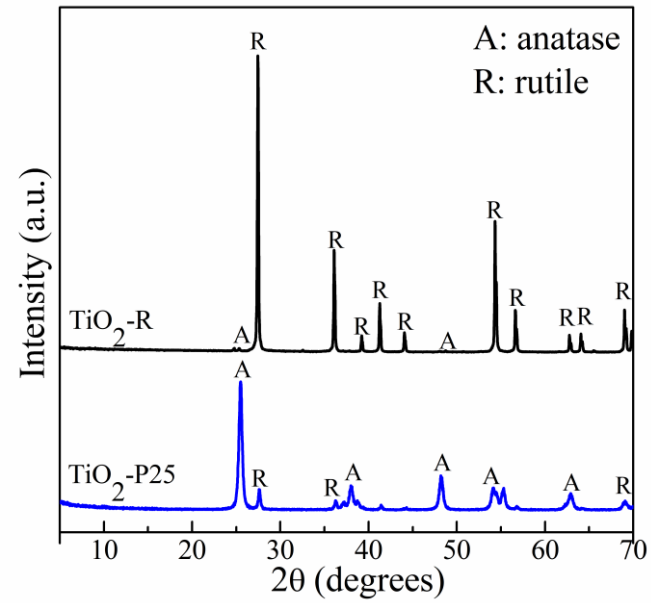

Fig. 1. X-ray diffractograms of studied samples.

TABLE I
CRYSTALLITE SIZE, S_{BET}, AND BAND GAP VALUES OF THE STUDIED SAMPLES.

Sample	Crystallite size (nm)	S_{BET} (m^2 g^{-1})	Band gap (eV)
TiO_2-P25	20[a]	51	3,2
TiO_2-R	6[b]	41	2,9

[a] calculated from the (101) crystallographic plane.
[b] calculated from the (110) crystallographic plane.

Fig. 2 shows the N_2 adsorption/desorption isotherms of the photocatalysts under study. Both materials exhibit adsorption isotherms that can be classified as type II, according to IUPAC [33]. In addition, the desorption isotherm of TiO_2-P25 presents a small hysteresis at high relative pressures [31]. These results may be attributed to nitrogen condensation within interparticle macropores at P/P_0 higher than 0.8 [34]. A detailed BJH pore size distribution of TiO_2-P25 showed the predominance of mesopores, however, the material also contains micro and macropores [31]. Similarly, in the case of rutile, BJH pore size distribution (data not shown) also indicates a broad range of pore sizes from micro to macropores. Additionally, there are notable differences in the volume of nitrogen adsorbed which is substantially lower for TiO_2-R, indicating poor porosity in this sample. Regarding the S_{BET}, there is an inverse relationship with crystallite size, where the S_{BET} decreases as the crystallite size increases. This difference may be again related to variations in the synthesis method.

Fig. 3 shows the UV-vis DRS spectra of the photocatalysts under study. TiO_2-P25 exhibits absorption between 220 and 380 nm, with absorption between 230 and 280 nm corresponding to charge transfer between tetrahedral titanium (IV) and O^{2-}, and absorption between 260 and 350 nm corresponding to charge

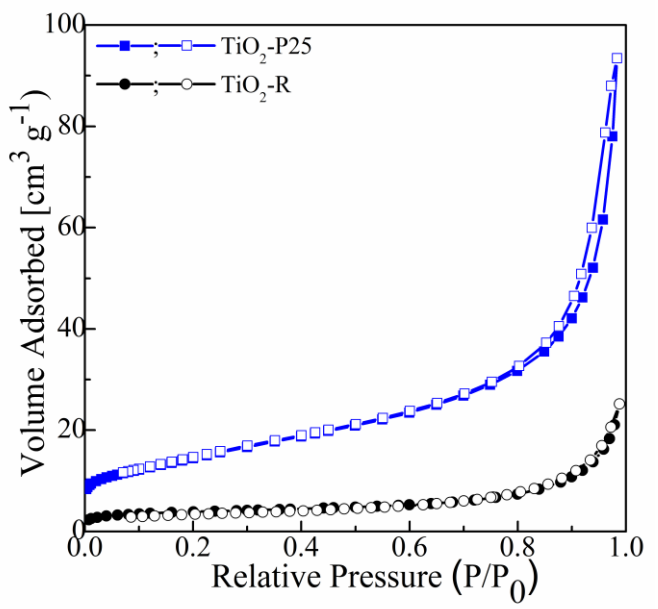

Fig. 2. N_2 adsorption-desorption isotherms of studied samples. Closed symbols represent adsorption curves and open symbols indicate desorption

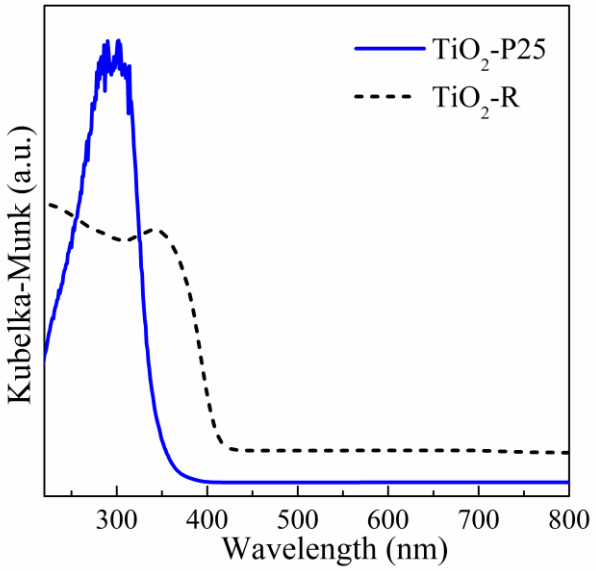

Fig. 3. UV-vis DRS spectra of studied samples.

transfer between octahedral (IV) titanium and O^{2-} sites [35]. For TiO_2-R, a strong absorption band is observed in the region between 220 and 400 nm, attributed to the band-to-band transition [18], [36], [37]. The calculated band gap values for TiO_2-P25 and TiO_2-R were 3.2 and 2.9 eV, respectively, closely correspond to the theoretical values [38], [39], [40]. The band gap is a crucial property of photocatalysts and directly impacts their catalytic performance. Electron-hole pairs are generated when the catalyst absorbs a photon whose energy meets or exceeds the band gap of the material [41]. On the other hand, if the band gap is too low, the excited light may not prevent electron-hole recombination, reducing photocatalytic performance [42].

B. *Photocatalysts activity over phenol degradation*

In the photolysis reactions, the solution was exposed solely

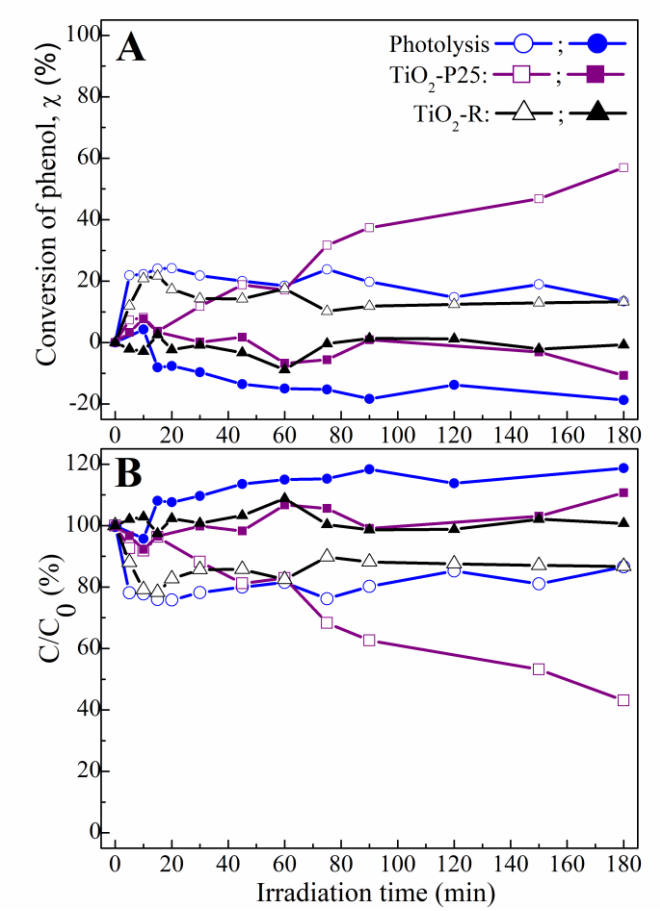

Fig. 4. Conversion of phenol (a) and C/C_0 (b) as a function of irradiation time
Open symbols: 9 W lamp tests; Closed symbols: 15 W lamp tests.

to ultraviolet light to assess the degradation of organic compound in the absence of a photocatalyst. In the photolysis of phenol under irradiation from a 9 W lamp, the conversion reached 22% in the first 5 min of the reaction (Fig. 4). Considering the deviation of the equipment, the conversion tended to remain stable up to 75 min of reaction, after which it began to decline from 90 min, oscillating until the end of the process. The decrease in conversion is related to an absorbance increase in the UV-vis spectrophotometer, leading to a higher concentration used in the calculations. This behavior suggests the formation of by-products that interfere with the assessment of degradation over irradiation time, likely due to the formation of intermediates such as catechol ($C_6H_6O_2$), hydroquinone ($C_6H_6O_2$), pyrogallol ($C_6H_6O_3$) and benzoquinone ($C_6H_4O_2$), which are molecules similar to phenol and that absorb radiation in the same wavelength range [43], [44], [45], [46]. Further supporting these observations, a color change in the phenol solution was noted during the reaction without a catalyst, indicating the formation of metabolites. In the case of phenol decomposition under irradiation of a 15 W lamp, the conversion was less pronounced, with negative conversion observed from the 60 min reaction. A color change in the phenol solution was also noted (Fig S1). This result can be attributed to a more pronounced formation of the intermediates during the process.

In the phenol degradation tests (Fig. 4), when the reactor was irradiated with a 9W lamp, phenol conversion using TiO_2-P25 was noticeable within the first 5 minutes of light exposure, gradually increasing to 57% after 180 min of reaction. For the TiO_2-R sample, phenol conversion reached 13% in the initial 5 min, rising to 23% in 15 min, then declining and stabilizing at 15% after 75 min of irradiation.

The anatase and rutile crystalline phases of TiO_2 absorb only ultraviolet rays, with the band gap of anatase being 3.2 eV, while that of the rutile phase is 2.9 eV [18]. Consequently, the TiO_2-rutile sample has a lower radiation absorption capacity, which reduces the number of free radicals available for phenol degradation and explains its low photocatalytic activity in the reaction under study [47]. In addition, the anatase phase has a high affinity for hydroxyl groups and a low rate of carrier recombination, resulting in greater efficiency in the generating reactive species, contributing to the more effective degradation of the pollutant [19]. This also explains the lower photocatalytic activity of TiO_2-R in the reaction under study.

Comparing the degradation of phenol in the presence of photocatalysts with that of the photolysis test for the 9W lamp, it is observed that the conversion tends to be slightly higher than that of the TiO_2-R sample. However, in the presence of the catalyst, there was no variation in the color of the reagent solution. This suggests that the presence of TiO_2-R can inhibit the formation of reaction intermediates.

In the photocatalytic degradation tests conducted under the 15 W lamp, negative conversions were observed regardless of the titanium dioxide used, with this effect being more pronounced for the TiO_2-P25 sample in the 180 min reaction. This unexpected result suggests that the increase in lamp power promotes the formation of reaction metabolites.

The photocatalytic degradation of phenol and TOC ratio (for the reaction effluents at 180 min) are presented in Table 2. Regardless of the lamp used it was observed that, even in cases where phenol conversion reached 56%, the TOC/TOC_0 ratio remained at 100%. This result indicates that despite the conversion of phenol, the total initial organic carbon remains in the reactive effluent, but in the form of other organic compounds. This finding supports the hypothesis that phenol is transformed into organic intermediates during the reaction.

TABLE II
PHENOL CONVERSION AND TOC/TOC_0 AFTER 180 MIN OF IRRADIATION.

Lamp	Sample	χ phenol (%)	TOC/TOC_0
9W	TiO_2-P25	56.9	100
	TiO_2-R	13.2	100
15 W	TiO_2-P25	-10.7	100
	TiO_2-R	-0.7	100

C. *Photocatalysts activity over MB degradation*

The results of MB photodegradation on TiO_2-P25 and TiO_2-R are shown in Fig. 5. In the photolysis reactions, the solution was exposed only to ultraviolet light to evaluate the degradation of methylene blue in the absence of a photocatalyst. As shown in Fig. 5, there was no considerable degradation of the pollutant during the 180 min exposure to the 9W germicidal lamp, as the dye conversion ranged between 2 and 5%, which is within the error margin of the equipment. Only about 2% of the pollutant was converted after 180 min. When the photolysis

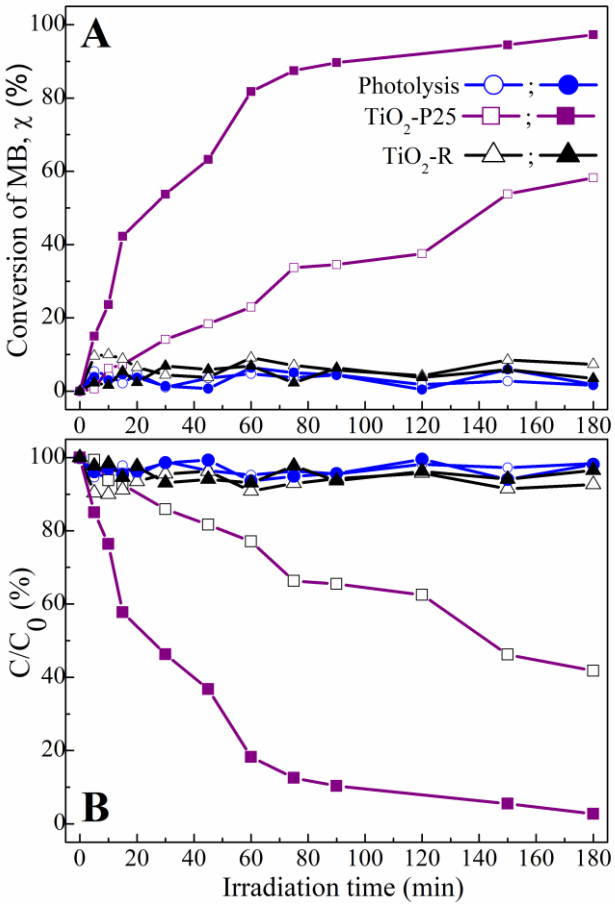

Fig. 5. Conversion of MB (a) and C/C_0 (b) as a function of irradiation time. Open symbol: 9 W lamp tests; Closed symbols: 15 W lamp tests.

of MB was evaluated using the 15W germicidal lamp, a behavior similar to that observed with the lower power lamp during 180 min reaction was noted.

Fig. 5 also presents the catalytic photodegradation of MB using the TiO_2-P25 photocatalyst under the 9 W germicidal lamp. This test demonstrated an expressive degradation of the contaminant, with a reduction in the concentration of approximately 35% over the first 75 min. The dye concentration continued to decrease, reaching about 42% of the initial value after 180 min of reaction. Thus, the total pollutant conversion observed was close to 58% by the end of the process, as shown in Fig. 5. In contrast, when evaluating the TiO_2-R photocatalyst under exposure to the 9W lamp, no degradation of the pollutant during the 180 min reaction, as shown in Fig. 5. Throughout the entire reaction, the MB conversion ranged from 4 to 10% with fluctuations within this range. The dye conversion achieved was approximately 7% in 180 min.

Comparing the crystalline phases of titania confirms that the photocatalytic activity for the degradation of MB with TiO_2-P25 is superior to that presented by TiO_2-R. The 58% dye conversion in 180 min with TiO_2-P25, compared to 7% of conversion obtained with TiO_2-R, can be attributed to the predominance of the anatase phase in TiO_2-P25. The anatase phase exhibits a high affinity for hydroxyl groups and a low rate of carrier recombination, which results in greater efficiency in the generating reactive species, thus enhancing the degradation of the pollutant [18].

When TiO_2-P25 was irradiated with the 15 W germicidal lamp, a pronounced degradation of MB was observed, especially in the initial 60 min, with a reduction in the initial concentration of approximately 95% (Fig. 5b). This decrease continued, resulting in a 97% conversion after 180 min, as shown in Fig. 5. In contrast, with the TiO_2-R photocatalyst under exposure to the 15 W lamp, the dye concentration in the solution remained close to the initial value throughout the reaction (Fig. 5b). After 180 min of reaction, only about 3% of MB was converted. Again TiO_2-P25 demonstrated to be more effective in generating the reactive species required for MB degradation. The higher radiation intensity provided by the 15 W lamp further improved this efficiency, leading to a more accelerated pollutant degradation.

When titania samples consisting exclusively of anatase or rutile crystalline phases were evaluated for the degradation of MB, anatase was found to show higher activity under both ultraviolet and visible light irradiation. This enhanced activity is attributed to the greater S_{BET} of the anatase compared to samples containing only the rutile phase. According to the N_2 adsorption-desorption analyses, the larger surface area of the anatase (whether pure or doped) contributes to its higher activity compared to rutile [48]. The high S_{BET} contributes to a larger surface, enhancing light absorption and the generation of electron/hole pairs, which can be quickly used in the reaction, reducing recombination effects and minimizing mass transfer limitation. The literature also emphasizes the role of adsorbed pollutants in the reaction mechanism, indicating that the larger the surface area of the catalyst, the greater the number of adsorbed pollutants [41].

Considering the TOC/TOC_0 ratio for the effluents from the degradation of MB over TiO_2-R, as shown in Table 3, it is observed that the value remained close to 100%. This indicates that, although MB was converted, it was transformed into intermediate organic molecules that do not significantly reduce the organic carbon content of the solution. For TiO_2-P25 in the photocatalytic degradation tests, even though MB conversion was high, the reduction in the TOC/TOC_0 ratio (Table 3) was considerably lower. This result suggests that the process is generating complex organic by-products rather than achieving complete mineralization, leading to the accumulation of organic intermediates in the effluent. Thus, to achieve a more detailed understanding of the reaction mechanism, additional analytical techniques such as liquid chromatography coupled with mass spectrometry are required to detect and characterize these by-products.

TABLE III
MB CONVERSION AND TOC/TOC_0 AFTER 180 MIN OF IRRADIATION.

Lamp	Sample	χ phenol (%)	TOC/TOC_0
9W	TiO_2-P25	58.2	77.8
	TiO_2-R	7.3	100
15 W	TiO_2-P25	97.3	68.4
	TiO_2-R	-0.7	91.7

SUPPLEMENTARY MATERIALS

Fig. S1 illustrates the change in phenol solution color after 180 min of irradiation with a 15W UV lamp.

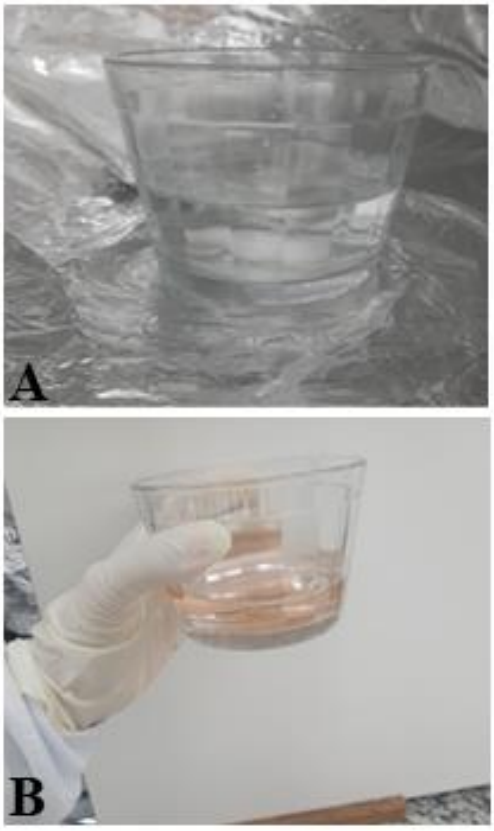

Fig. S1. Phenol solution at 100 ppm: (a) prior to 15W UV lamp irradiation; (b) after 180 min of 15W UV lamp irradiation.

ACKNOWLEDGMENT

The authors thank FAPEMIG for their financial support, the Multiuser Laboratory of Instrumental Analysis of the School of Engineering of the Federal University of Lavras (LABMAI/EENG/UFLA) for conducting TOC analyses, and the Research Center for Advanced Materials and Energy at the Federal University of São Carlos for performing XRD and N_2 adsorption-desorption analyses.

REFERENCES

[1] A. S. Perera *et al.*, "A non-doped microporous titanosilicate for bimodal adsorption-photocatalysis based removal of organic water pollutants," *Microporous and Mesoporous Materials*, vol. 345, p. 112276, Nov. 2022, doi: 10.1016/j.micromeso.2022.112276.

[2] M. Syafrudin *et al.*, "Pesticides in Drinking Water—A Review," *Int J Environ Res Public Health*, vol. 18, no. 2, p. 468, Jan. 2021, doi: 10.3390/ijerph18020468.

[3] M.-C. Danner, A. Robertson, V. Behrends, and J. Reiss, "Antibiotic pollution in surface fresh waters: Occurrence and effects," *Science of The Total Environment*, vol. 664, pp. 793–804, May 2019, doi: 10.1016/j.scitotenv.2019.01.406.

[4] U. Shanker, M. Rani, and V. Jassal, "Degradation of hazardous organic dyes in water by nanomaterials," *Environ Chem Lett*, vol. 15, no. 4, pp. 623–642, Dec. 2017, doi: 10.1007/s10311-017-0650-2.

[5] O. M. Ogunbanwo *et al.*, "High Concentrations of Pharmaceuticals in a Nigerian River Catchment," *Environ Toxicol Chem*, vol. 41, no. 3, pp. 551–558, Mar. 2022, doi: 10.1002/etc.4879.

[6] A. Bibi, S. Bibi, M. Abu-Dieyeh, and M. A. Al-Ghouti, "Towards sustainable physiochemical and biological techniques for the remediation of phenol from wastewater: A review on current applications and removal mechanisms," *J Clean Prod*, vol. 417, p. 137810, Sep. 2023, doi: 10.1016/j.jclepro.2023.137810.

[7] A. Almasi, M. Mahmoudi, M. Mohammadi, A. Dargahi, and H. Biglari, "Optimizing biological treatment of petroleum industry wastewater in a facultative stabilization pond for simultaneous removal of carbon and phenol," *Toxin Rev*, vol. 40, no. 2, pp. 189–197, Apr. 2021, doi: 10.1080/15569543.2019.1573433.

[8] A. Mohd, "Presence of phenol in wastewater effluent and its removal: an overview," *Int J Environ Anal Chem*, vol. 102, no. 6, pp. 1362–1384, May 2022, doi: 10.1080/03067319.2020.1738412.

[9] I. Khan *et al.*, "Review on Methylene Blue: Its Properties, Uses, Toxicity and Photodegradation," *Water (Basel)*, vol. 14, no. 2, p. 242, Jan. 2022, doi: 10.3390/w14020242.

[10] A. S. Eltaweil, G. S. Elgarhy, G. M. El-Subruiti, and A. M. Omer, "Carboxymethyl cellulose/carboxylated graphene oxide composite microbeads for efficient adsorption of cationic methylene blue dye," *Int J Biol Macromol*, vol. 154, pp. 307–318, Jul. 2020, doi: 10.1016/j.ijbiomac.2020.03.122.

[11] J. Wang and S. Wang, "Reactive species in advanced oxidation processes: Formation, identification and reaction mechanism," *Chemical Engineering Journal*, vol. 401, p. 126158, Dec. 2020, doi: 10.1016/j.cej.2020.126158.

[12] M. Z. Akbari, Y. Xu, Z. Lu, and L. Peng, "Review of antibiotics treatment by advance oxidation processes," *Environmental Advances*, vol. 5, p. 100111, Oct. 2021, doi: 10.1016/j.envadv.2021.100111.

[13] J. Iyyappan, B. Gaddala, R. Gnanasekaran, M. Gopinath, D. Yuvaraj, and V. Kumar, "Critical review on wastewater treatment using photo catalytic advanced oxidation process: Role of photocatalytic materials, reactor design and kinetics," *Case Studies in Chemical and Environmental Engineering*, vol. 9, p. 100599, Jun. 2024, doi: 10.1016/j.cscee.2023.100599.

[14] G. Veréb *et al.*, "Highly efficient bacteria inactivation and phenol degradation by visible light irradiated iodine doped TiO_2," *Appl Catal B*, vol. 129, pp. 194–201, Jan. 2013, doi: 10.1016/j.apcatb.2012.08.037.

[15] S.-W. Lv, Y. Cong, X. Chen, W. Wang, and L. Che, "Developing fine-tuned metal–organic frameworks for

photocatalytic treatment of wastewater: A review," *Chemical Engineering Journal*, vol. 433, p. 133605, Apr. 2022, doi: 10.1016/j.cej.2021.133605.

[16] M. R. Al-Mamun, S. Kader, M. S. Islam, and M. Z. H. Khan, "Photocatalytic activity improvement and application of UV-TiO_2 photocatalysis in textile wastewater treatment: A review," *J Environ Chem Eng*, vol. 7, no. 5, p. 103248, Oct. 2019, doi: 10.1016/j.jece.2019.103248.

[17] Y. Li, X. Li, J. Li, and J. Yin, "Photocatalytic degradation of methyl orange by TiO_2-coated activated carbon and kinetic study," *Water Res*, vol. 40, no. 6, pp. 1119–1126, Mar. 2006, doi: 10.1016/j.watres.2005.12.042.

[18] J. Zhang, P. Zhou, J. Liu, and J. Yu, "New understanding of the difference of photocatalytic activity among anatase, rutile and brookite TiO_2," *Physical Chemistry Chemical Physics*, vol. 16, no. 38, pp. 20382–20386, 2014, doi: 10.1039/C4CP02201G.

[19] Md. B. K. Suhan *et al.*, "Sustainable pollutant removal and wastewater remediation using TiO_2-based nanocomposites: A critical review," *Nano-Structures & Nano-Objects*, vol. 36, p. 101050, Oct. 2023, doi: 10.1016/j.nanoso.2023.101050.

[20] A. K. Chakraborty, S. Akter, S. Ganguli, M. A. Haque, A. S. M. Nur, and M. A. Sabur, "Design of $FeWO_4$@N-TiO2 nanocomposite and its enhanced photocatalytic activity in decomposing methylene blue and phenol under visible light," *Environ Technol Innov*, p. 103536, Jan. 2024, doi: 10.1016/j.eti.2024.103536.

[21] S. Mishra, N. Chakinala, A. G. Chakinala, and P. K. Surolia, "Photocatalytic degradation of methylene blue using monometallic and bimetallic Bi-Fe doped TiO_2," *Catal Commun*, vol. 171, p. 106518, Nov. 2022, doi: 10.1016/j.catcom.2022.106518.

[22] T. Z. Liza, M. M. H. Tusher, F. Anwar, M. F. Monika, K. F. Amin, and F. N. U. Asrafuzzaman, "Effect of Ag-doping on morphology, structure, band gap and photocatalytic activity of bio-mediated TiO_2 nanoparticles," *Results in Materials*, vol. 22, p. 100559, Jun. 2024, doi: 10.1016/j.rinma.2024.100559.

[23] A. K. Behera, K. P. Shadangi, and P. K. Sarangi, "Synthesis of dye-sensitized TiO_2/Ag doped nano-composites using UV photoreduction process for phenol degradation: A comparative study," *Environmental Pollution*, vol. 312, p. 120019, Nov. 2022, doi: 10.1016/j.envpol.2022.120019.

[24] Y. Liu, S. Zhou, F. Yang, H. Qin, and Y. Kong, "Degradation of phenol in industrial wastewater over the F–Fe/TiO_2 photocatalysts under visible light illumination," *Chin J Chem Eng*, vol. 24, no. 12, pp. 1712–1718, Dec. 2016, doi: 10.1016/j.cjche.2016.05.024.

[25] Y. J. O. Asencios, V. S. Lourenço, and W. A. Carvalho, "Removal of phenol in seawater by heterogeneous photocatalysis using activated carbon materials modified with TiO_2," *Catal Today*, vol. 388–389, pp. 247–258, Apr. 2022, doi: 10.1016/j.cattod.2020.06.064.

[26] Y. Yue *et al.*, "Synergistic adsorption and photocatalysis study of TiO_2 and activated carbon composite," *Heliyon*, vol. 10, no. 10, p. e30817, May 2024, doi: 10.1016/j.heliyon.2024.e30817.

[27] A. L. Patterson, "The Scherrer Formula for X-Ray Particle Size Determination," *Physical Review*, vol. 56, no. 10, pp. 978–982, Nov. 1939, doi: 10.1103/PhysRev.56.978.

[28] S. Brunauer, P. H. Emmett, and E. Teller, "Adsorption of Gases in Multimolecular Layers," *J Am Chem Soc*, vol. 60, no. 2, pp. 309–319, Feb. 1938, doi: 10.1021/ja01269a023.

[29] R. S. Weber, "Effect of Local Structure on the UV-Visible Absorption Edges of Molybdenum Oxide Clusters and Supported Molybdenum Oxides," *J Catal*, vol. 151, no. 2, pp. 470–474, Feb. 1995, doi: 10.1006/jcat.1995.1052.

[30] D. Sarkar, S. Mukherjee, and K. K. Chattopadhyay, "Synthesis, characterization and high natural sunlight photocatalytic performance of cobalt doped TiO_2 nanofibers," *Physica E Low Dimens Syst Nanostruct*, vol. 50, pp. 37–43, May 2013, doi: 10.1016/j.physe.2013.02.010.

[31] C. A. Sierra-Pereira and E. A. Urquieta-González, "Reduction of NO with CO on CuO or Fe_2O_3 catalysts supported on TiO_2 in the presence of O_2, SO_2 and water steam," *Fuel*, vol. 118, pp. 137–147, Feb. 2014, doi: 10.1016/j.fuel.2013.10.054.

[32] W. M. Shaheen, "Thermal solid–solid interaction and catalytic properties of CuO/Al_2O_3 system treated with ZnO and MoO3," *Thermochim Acta*, vol. 385, no. 1–2, pp. 105–116, Mar. 2002, doi: 10.1016/S0040-6031(01)00710-9.

[33] M. Thommes *et al.*, "Physisorption of gases, with special reference to the evaluation of surface area and pore size distribution (IUPAC Technical Report)," *Pure and Applied Chemistry*, vol. 87, no. 9–10, pp. 1051–1069, Oct. 2015, doi: 10.1515/pac-2014-1117.

[34] G. V. Oliveira, V. de Macedo, E. A. Urquieta-González, Z. M. Magriotis, and C. A. Pereira, "Fe_2O_3/γ-Al_2O_3 and NiO/γ-Al_2O_3 catalysts for the selective catalytic oxidation of ammonia," *Catal Today*, vol. 444, p. 114991, Jan. 2025, doi: 10.1016/j.cattod.2024.114991.

[35] H. Nur, "Modification of titanium surface species of titania by attachment of silica nanoparticles," *Materials Science and Engineering: B*, vol. 133, no. 1–3, pp. 49–54, Aug. 2006, doi: 10.1016/j.mseb.2006.05.003.

[36] E. Wang, T. He, L. Zhao, Y. Chen, and Y. Cao, "Improved visible light photocatalytic activity of titania doped with tin and nitrogen," *J. Mater. Chem.*, vol. 21, no. 1, pp. 144–150, 2011, doi: 10.1039/C0JM02539A.

[37] B. Gao, Y. Ma, Y. Cao, W. Yang, and J. Yao, "Great Enhancement of Photocatalytic Activity of Nitrogen-Doped Titania by Coupling with Tungsten Oxide," *J Phys Chem B*, vol. 110, no. 29, pp. 14391–14397, Jul. 2006, doi: 10.1021/jp0624606.

[38] S. Majumder, D. Paramanik, V. Solanki, B. P. Bag, and S. Varma, "Bandgap tailoring of rutile TiO_2(110) via surface patterning with electron cyclotron resonance

sputtering," *Appl Phys Lett*, vol. 98, no. 5, Jan. 2011, doi: 10.1063/1.3549768.

[39] K. Yang, Y. Dai, B. Huang, and S. Han, "Theoretical Study of N-Doped TiO_2 Rutile Crystals," *J Phys Chem B*, vol. 110, no. 47, pp. 24011–24014, Nov. 2006, doi: 10.1021/jp0651135.

[40] L. Sun, J. Li, C. L. Wang, S. F. Li, H. B. Chen, and C. J. Lin, "An electrochemical strategy of doping Fe^{3+} into TiO_2 nanotube array films for enhancement in photocatalytic activity," *Solar Energy Materials and Solar Cells*, vol. 93, no. 10, pp. 1875–1880, Oct. 2009, doi: 10.1016/j.solmat.2009.07.001.

[41] M. Faisal, S. B. Khan, M. M. Rahman, A. Jamal, A. M. Asiri, and M. M. Abdullah, "Smart chemical sensor and active photo-catalyst for environmental pollutants," *Chemical Engineering Journal*, vol. 173, no. 1, pp. 178–184, Sep. 2011, doi: 10.1016/j.cej.2011.07.067.

[42] D. Chen *et al.*, "Photocatalytic degradation of organic pollutants using TiO_2-based photocatalysts: A review," *J Clean Prod*, vol. 268, p. 121725, Sep. 2020, doi: 10.1016/j.jclepro.2020.121725.

[43] H. Chun, W. Yizhong, and T. Hongxiao, "Destruction of phenol aqueous solution by photocatalysis or direct photolysis," *Chemosphere*, vol. 41, no. 8, pp. 1205–1209, Oct. 2000, doi: 10.1016/S0045-6535(99)00539-1.

[44] J. Araña, E. Tello Rendón, J. M. Doña Rodríguez, J. A. Herrera Melián, O. González Díaz, and J. Pérez Peña, "Highly concentrated phenolic wastewater treatment by the Photo-Fenton reaction, mechanism study by FTIR-ATR," *Chemosphere*, vol. 44, no. 5, pp. 1017–1023, Aug. 2001, doi: 10.1016/S0045-6535(00)00359-3.

[45] J. Chen, L. Eberlein, and C. H. Langford, "Pathways of phenol and benzene photooxidation using TiO_2 supported on a zeolite," *J Photochem Photobiol A Chem*, vol. 148, no. 1–3, pp. 183–189, May 2002, doi: 10.1016/S1010-6030(02)00041-2.

[46] M. Salaices, B. Serrano, and H. I. de Lasa, "Photocatalytic conversion of phenolic compounds in slurry reactors," *Chem Eng Sci*, vol. 59, no. 1, pp. 3–15, Jan. 2004, doi: 10.1016/j.ces.2003.07.015.

[47] M. Qamar, M. Muneer, and D. Bahnemann, "Heterogeneous photocatalysed degradation of two selected pesticide derivatives, triclopyr and daminozid in aqueous suspensions of titanium dioxide," *J Environ Manage*, vol. 80, no. 2, pp. 99–106, Jul. 2006, doi: 10.1016/j.jenvman.2005.09.002.

[48] M. R. Elahifard, S. Ahmadvand, and A. Mirzanejad, "Effects of Ni-doping on the photo-catalytic activity of TiO_2 anatase and rutile: Simulation and experiment," *Mater Sci Semicond Process*, vol. 84, pp. 10–16, Sep. 2018, doi: 10.1016/j.mssp.2018.05.001.